Asociación Argentina
de Mecánica Computacional

Mecánica Computacional Vol XXX, págs. 3107-3124 (artículo completo)
Oscar Möller, Javier W. Signorelli, Mario A. Storti (Eds.)
Rosario, Argentina, 1-4 Noviembre 2011

REDUCED ORDER MODEL FORMULATION FOR THE STUDY OF THE FREE AND FORCED RESPONSE OF A MISTUNED IMPELLER WITH TWO BLADE GEOMETRIES

Luis A. Boulton[a] , **Euro Casanova**[b]

Departamento de Mecánica, Universidad Simón Bolívar, Apdo. 89000, Caracas 1080A, Venezuela,
[a]*laboulton@gmail.com*
[b]*ecasanov@usb.ve, http://prof.usb.ve/ecasanov*

Keywords: Reduced order model, mistuning, impeller, blade geometry.

Abstract. Numerous works have presented techniques for obtaining reduced order models (ROMs) of mistuned bladed disks. Most of these works focus in only one rotor's stage, though some also include several stages and even the rotor shaft. However, to the authors' knowledge, the ROM techniques presented consider only one blade geometry by stage. This paper shows an adaptation of a previously published reduced order modelling technique in order to allow its application to the case of an impeller incorporating two different blade geometries (main and splitter blade). The technique is based in Craig and Bampton's component mode synthesis, and it permits to introduce different mistuning patterns for each blade geometry, while the disk is considered as a cyclic symmetric structure.
The proposed technique is applied to an impeller's simplified model, in order to assess its precision and validity. Validation is carried out by comparison of predictions for the free and forced response of the mistuned impeller, obtained by means of the ROM and the finite element parent model. Results show that the ROM properly represents the dynamic features of the parent model in the frequency range of interest, with minimal computational cost. Furthermore, the ROM properly captures the localization phenomenon when it occurs, in both, the normal modes and the forced response.

1 INTRODUCTION

The small inevitable variations (uncertainties) in the structural properties, material properties and blade geometries of bladed disks, caused by manufacturing tolerances and wear during operation, are referred as mistuning. These uncertainties, coupled with flexibility of the disk, can produce a large deviation in blade vibration amplitudes (localization phenomena) compared to the fully symmetrical (tuned) bladed disk. As a consequence, the cyclic symmetry is lost and a sector analysis cannot be performed, therefore imposing the modeling of the entire bladed disk geometry which is computationally expensive.

Mistuning in bladed disks depends on many factors and it is difficult to quantify in a deterministic manner, imposing statistical analyses for predicting the dynamic response of these structures. Statistical analyses are computationally intensive tasks that can easily become infeasible due to the large size of the finite element models involved. If mistuning is to be considered, reduced-order models have to be used to predict a dynamic response.

Some researchers have focused on the development of reduced-order models for the vibration analysis of single stage mistuned rotors (Bladh et al., 2001; Casanova, 2002; Petrov et al., 2003) or multi stage mistuned rotors (Song ,2005; Laxalde, 2007; Sinha, 2007; Boulton and Casanova, 2009); nevertheless, most of the models presented in the literature are focused on axial-flow turbomachines, which are perceived to be important in applications such as aircraft propulsion. On the other hand, Ziaei-Rad (2005) worked with one impeller geometry to investigate the vibration of a typical radial-flow turbomachine with a tapered blade, but no reduced-order model or mistuning was considered. Patel et al. (2004) also studied an impeller to investigate its response to structural mistuning; a reduced-order model was obtained from an industrial rotor using the Turbo-Reduced code, and blade mistuning analysis was performed, however no splitter blades were reported.

In the present paper, a new reduced-order model is developed to study the dynamics of a mistuned impeller having splitter blades, and permitting to impose different mistuning patterns for the main and the splitter blades. This procedure is based on the classical Craig and Bampton (1968) component mode synthesis method. The main blades, the splitter blades and the disk are modeled as separate components. The disk is modeled exploiting the cyclic symmetry. Validation is done comparing the reduced-order model and the parent finite element model for free and forced response of the tuned and mistuned impeller.

2 REDUCED ORDER MODELLING TECHNIQUE

The reduced order modeling technique implemented in this paper is based on a methodology previously published by Casanova (2002) and Seguí and Casanova (2006). This methodology makes uses of a Craig and Bampton (1968) component mode synthesis (CMS) formulated specifically for the analysis of mistuned bladed disks considering or not the shaft. In this technique, each blade, the disk, and if relevant, the shaft, are considered as substructures. The mistuning is assumed to be located only in the blades, thus permitting to consider the disk as a cyclic symmetric substructure. In this work this technique has been extended in order to be able to address the problems of impellers where two or more blade types are mounted on the same disk.

Only the finite element mass and stiffness matrices from a blade of each type, and from a disk sector are necessary to construct the reduced matrices for the whole impeller (*cf*. Figure 1).

(a) (b)

Figure 1: Sector of Impeller: a) frontal view; b) isometric view)

2.1 Blade modeling

To obtain the ROM of the impeller all the blades of the same type are considered equal, therefore it is only necessary to have the mass and stiffness matrices of a blade representing each blade type of the impeller. Mistuning will be introduced once the ROM is fully formulated.

For each blade type, the blade DOFs are partitioned in internal DOFs (*C*) and interface DOFs (*I*), so the stiffness finite element (FE) matrix for blade type *i* has the form (mass matrix is ordered in analogous form):

$$\mathbf{K}^{A_i} = \begin{bmatrix} \mathbf{K}_{CC}^{A_i} & \mathbf{K}_{CI}^{A_i} \\ \mathbf{K}_{IC}^{A_i} & \mathbf{K}_{II}^{A_i} \end{bmatrix} \tag{1}$$

In this expression and hereafter, the superscript A_i represent terms related to the blade of type *i*. The blade DOFs may be expressed in a reduced set of modal coordinates using Craig and Bampton (1968) formulation:

$$\mathbf{u}^{A_i} = \begin{Bmatrix} \mathbf{u}_C^{A_i} \\ \mathbf{u}_I^{A_i} \end{Bmatrix} = \begin{bmatrix} \Phi_{Cq}^{A_i} & \Psi_{CI}^{A_i} \\ \mathbf{0} & \mathbf{I}_I \end{bmatrix} \begin{Bmatrix} \mathbf{p}_q^{A_i} \\ \mathbf{p}_I^{A_i} \end{Bmatrix} = \mathbf{H}^{A_i}\, \mathbf{p}^{A_i} \tag{2}$$

Note that in this formulation the physical and modal coordinates representing the interface DOFs are the same, while the internal physical DOFs (*C*) are represented by a reduced set of modal coordinates (*q*). The block $\Psi_{CI}^{A_i} = -\left[\mathbf{K}_{CC}^{A_i}\right]^{-1}\mathbf{K}_{CI}^{A_i}$ represent a set of *I* static constraint modes, while $\Phi_{Cq}^{A_i} = \left[\boldsymbol{\varphi}_{C1}^{A_i} \cdots \boldsymbol{\varphi}_{Cq}^{A_i}\right]$ represent a set of *q* fixed interface normal modes, *i.e.* the cantilevered blade modes, which are computed from the eigenproblem:

$$\mathbf{K}_{CC}^{A_i}\boldsymbol{\varphi}_{Cr}^{A_i} = \omega_r^2 \mathbf{M}_{CC}^{A_i}\boldsymbol{\varphi}_{Cr}^{A_i} \qquad r = 1, \cdots, q \tag{3}$$

Projecting the blade mass and stiffness matrices in the corresponding blade modal basis gives the reduced modal mass and stiffness matrices for each blade type:

$$\mathbf{k}^{A_i} = \left[\mathbf{H}^{A_i}\right]^T \mathbf{K}^{A_i}\, \mathbf{H}^{A_i} = \begin{bmatrix} \Lambda_q^{A_i} & \mathbf{0} \\ sym & \mathbf{k}_{II}^{A_i} \end{bmatrix} \quad , \quad \mathbf{m}^{A_i} = \left[\mathbf{H}^{A_i}\right]^T \mathbf{M}^{A_i}\, \mathbf{H}^{A_i} = \begin{bmatrix} \mathbf{I}_{q_i} & \mathbf{m}_{qI}^{A_i} \\ sym & \mathbf{m}_{II}^{A_i} \end{bmatrix} \tag{4}$$

Where:

$$\begin{aligned}
\Lambda_q^{A_i} &= \mathrm{diag}\left(\omega_1^2,\cdots,\omega_q^2\right)_i \\
\mathbf{k}_{II}^{A_i} &= \mathbf{K}_{II}^{A_i} + \mathbf{K}_{IC}^{A_i}\Psi_{CI}^{A_i} \\
\mathbf{m}_{qI}^{A_i} &= \left[\Phi_{Cq}^{A_i}\right]^T\left[\mathbf{M}_{CC}^{A_i}\Psi_{CI}^{A_i} + \mathbf{M}_{CI}^{A_i}\right] \\
\mathbf{m}_{II}^{A_i} &= \left[\Psi_{CI}^{A_i}\right]^T\left[\mathbf{M}_{CC}^{A_i}\Psi_{CI}^{A} + \mathbf{M}_{CI}^{A_i}\right] + \mathbf{M}_{IC}^{A_i}\Psi_{CI}^{A_i} + \mathbf{M}_{II}^{A_i}
\end{aligned} \tag{5}$$

Finally, ordering the modal coordinates for all the blades of the impeller according to:

$$\mathbf{p}^{\mathcal{A}} = \left[\begin{Bmatrix}\mathbf{p}_{q_1}^{A_1}\\ \mathbf{p}_{q_2}^{A_2}\end{Bmatrix}_{j=1}^{T} \cdots \begin{Bmatrix}\mathbf{p}_{q_1}^{A_1}\\ \mathbf{p}_{q_2}^{A_2}\end{Bmatrix}_{j=N}^{T} \begin{Bmatrix}\mathbf{p}_{I_1}^{A_1}\\ \mathbf{p}_{I_2}^{A_2}\end{Bmatrix}_{j=1}^{T} \cdots \begin{Bmatrix}\mathbf{p}_{I_1}^{A_1}\\ \mathbf{p}_{I_2}^{A_2}\end{Bmatrix}_{j=N}^{T}\right]^T \tag{6}$$

permits to express the stiffness and mass matrices for all the blades of the impeller (denoted with the calligraphic superscript $\mathcal{A}$) as:

$$\mathbf{k}^{\mathcal{A}} = \begin{bmatrix}\Lambda_Q^{\mathcal{A}} & \mathbf{0}\\ \mathbf{0} & \mathbf{k}_{YY}^{\mathcal{A}}\end{bmatrix} \quad , \quad \mathbf{m}^{\mathcal{A}} = \begin{bmatrix}\mathbf{I}_Q & \mathbf{m}_{QY}^{\mathcal{A}}\\ sym & \mathbf{m}_{YY}^{\mathcal{A}}\end{bmatrix} \tag{7}$$

where block matrices expressions are given by:

$$\Lambda_Q^{\mathcal{A}} = \mathbf{I}_N \otimes \begin{bmatrix}\Lambda_{q_1}^{A_1} & \mathbf{0}\\ \mathbf{0} & \Lambda_{q_2}^{A_2}\end{bmatrix} \quad , \quad \mathbf{k}_{YY}^{\mathcal{A}} = \mathbf{I}_N \otimes \begin{bmatrix}\mathbf{k}_{I_1I_1}^{A_1} & \mathbf{0}\\ \mathbf{0} & \mathbf{k}_{I_2I_2}^{A_2}\end{bmatrix} \tag{8}$$

$$\mathbf{m}_{QY}^{\mathcal{A}} = \mathbf{I}_Q \otimes \begin{bmatrix}\mathbf{m}_{q_1I_1}^{A_1} & \mathbf{0}\\ \mathbf{0} & \mathbf{m}_{q_2I_2}^{A_2}\end{bmatrix} \quad , \quad \mathbf{m}_{YY}^{\mathcal{A}} = \mathbf{I}_Q \otimes \begin{bmatrix}\mathbf{m}_{I_1I_1}^{A_1} & \mathbf{0}\\ \mathbf{0} & \mathbf{m}_{I_2I_2}^{A_2}\end{bmatrix} \tag{9}$$

In these expressions, the symbol $\otimes$ denotes the Kronecker product, $Q = N(q_1 + q_2)$ and $Y = N(I_1 + I_2)$.

2.2 Disk modeling

As mentioned before, the disk is considered to be a cyclic symmetric structure; therefore the disk model may be obtained by means of cyclic symmetry, using exclusively the mass and stiffness matrices of a disk sector. This formulation is based on the work of Casanova (2002) and is only briefly presented here to show the differences of including two blade types in each disk sector.

The global disk stiffness matrix $\mathbf{K}^{\mathcal{D}}$ can be obtained by means of the global disk stiffness matrix expressed in the space of real cyclic coordinates $\widetilde{\mathbf{K}}^{\mathcal{D}}$ (the procedure is analogous for the mass matrix and is not presented here for the sake of space):

$$\mathbf{K}^{\mathcal{D}} = \left(\mathbf{F}_N \otimes \mathbf{I}_m\right)\widetilde{\mathbf{K}}^{\mathcal{D}}\left(\mathbf{F}_N^T \otimes \mathbf{I}_m\right) \tag{10}$$

Where N is the number of sectors in the structure, m is the size of a disk sector matrix and $\mathbf{F}_N$ is the real-valued Fourier matrix of size N, defined as:

$$\mathbf{F}_N = \sqrt{\frac{2}{N}} \begin{bmatrix} \frac{1}{\sqrt{2}} & 1 & 0 & \cdots & 0 & 1 & \frac{1}{\sqrt{2}} \\ \frac{1}{\sqrt{2}} & \cos(\alpha) & \sin(\alpha) & \cdots & \cos((W-1)\alpha) & \sin((W-1)\alpha) & \frac{-1}{\sqrt{2}} \\ \frac{1}{\sqrt{2}} & \cos(2\alpha) & \sin(2\alpha) & \cdots & \cos((W-1)2\alpha) & \sin((W-1)2\alpha) & \frac{1}{\sqrt{2}} \\ \vdots & \vdots & \vdots & & \vdots & \vdots & \vdots \\ \frac{1}{\sqrt{2}} & \cos((N-1)\alpha) & \sin((N-1)\alpha) & \cdots & \cos((W-1)(N-1)\alpha) & \sin((W-1)(N-1)\alpha) & \frac{(-1)^{N-1}}{\sqrt{2}} \end{bmatrix} \tag{11}$$

With $\alpha = 2\pi/N$ the sector angle, and $W = \text{int}[(N+1)/2]$ the highest possible harmonic. Note that the last column of this matrix exists only if N is even.

Hereafter the calligraphic superscript $\mathcal{D}$ is used to denote the whole disk matrices, while the superscript D is used to denote matrices related to the disk sector. Likewise, the "tilde" notation denotes matrices expressed in the real cyclic coordinate space.

The stiffness matrix in real cyclic coordinates is a pseudo-block diagonal matrix of the form:

$$\widetilde{\mathbf{K}}^{\mathcal{D}} = \begin{bmatrix} \widetilde{\mathbf{K}}_m^{D_1} & & & & \\ & \widetilde{\mathbf{K}}_{2m}^{D_2} & & & \\ & & \ddots & & \\ & & & \widetilde{\mathbf{K}}_{2m}^{D_W} & \\ & & & & \widetilde{\mathbf{K}}_m^{D_W} \end{bmatrix} \tag{12}$$

Where $\widetilde{\mathbf{K}}_m^{D_j}$ and $\widetilde{\mathbf{K}}_{2m}^{D_j}$ represent blocks for single harmonics (m) and double harmonics ($2m$), respectively. (Note that block $\widetilde{\mathbf{K}}_m^{D_W}$ only exists if N is even). It can be demonstrated that all these blocks are function of the terms of a single sector stiffness matrix, as will be shown shortly. In order to facilitate the description, the DOFs of a disk sector is partitioned in internal DOFs (C), right interface DOFs (R), left interface DOFs (L), and blade-disk interface DOFs for blade 1 and blade 2 (I_1, I_2). With this partitioning, the stiffness matrix (of dimension m) of a disk sector is expressed as:

$$\mathbf{K}^D = \begin{bmatrix} \mathbf{K}_{CC}^D & \mathbf{K}_{CL}^D & \mathbf{K}_{CR}^D & \mathbf{K}_{CI_1}^D & \mathbf{K}_{CI_2}^D \\ & \mathbf{K}_{LL}^D & \mathbf{K}_{LR}^D & \mathbf{K}_{LI_1}^D & \mathbf{K}_{LI_2}^D \\ & & \mathbf{K}_{RR}^D & \mathbf{K}_{RI_1}^D & \mathbf{K}_{RI_2}^D \\ & & & \mathbf{K}_{I_1I_1}^D & \mathbf{K}_{I_1I_2}^D \\ \textit{sym} & & & & \mathbf{K}_{I_2I_2}^D \end{bmatrix} \tag{13}$$

In this formulation, the right interface DOFs (R) are chosen to be the dependent cyclic boundary and are therefore eliminated, and the internal (C) and left (L) DOFs are grouped into sector internal DOFs (χ). With these definitions, the double harmonics ($2m$) blocs present the following form:

$$\widetilde{\mathbf{K}}_{2m}^{D_j} = \begin{bmatrix} \widetilde{\mathbf{K}}_{\chi\chi}^{D_j} & \widetilde{\mathbf{K}}_{\chi I_1}^{D_j} & \widetilde{\mathbf{K}}_{\chi I_2}^{D_j} \\ & \widetilde{\mathbf{K}}_{I_1I_1}^{D_j} & \widetilde{\mathbf{K}}_{I_1I_2}^{D_j} \\ \textit{sym} & & \widetilde{\mathbf{K}}_{I_2I_2}^{D_j} \end{bmatrix} \tag{14}$$

Where the sector internal partition $\widetilde{\mathbf{K}}_{\chi\chi}^{D_j}$ of Eq. (11) takes the following form:

$$\widetilde{\mathbf{K}}_{\chi\chi}^{D_j} = \begin{bmatrix} \hat{\mathbf{K}}_C + \left[\hat{\mathbf{K}}_R + \hat{\mathbf{K}}_L\right]\cos\left((j-1)\alpha\right) & \left[\hat{\mathbf{K}}_R - \hat{\mathbf{K}}_L\right]\sin\left((j-1)\alpha\right) \\ -\left[\hat{\mathbf{K}}_R - \hat{\mathbf{K}}_L\right]\sin\left((j-1)\alpha\right) & \hat{\mathbf{K}}_C + \left[\hat{\mathbf{K}}_R + \hat{\mathbf{K}}_L\right]\cos\left((j-1)\alpha\right) \end{bmatrix} \tag{15}$$

With:

$$\hat{\mathbf{K}}_C = \begin{bmatrix} \mathbf{K}_{CC}^D & \mathbf{K}_{CL}^D \\ \mathbf{K}_{LC}^D & \mathbf{K}_{LL}^D + \Gamma_{RL}^T \mathbf{K}_{RR}^D \Gamma_{RL} \end{bmatrix} \quad , \quad \hat{\mathbf{K}}_R = \begin{bmatrix} \mathbf{0} & \mathbf{K}_{CR}^D \Gamma_{RL} \\ \mathbf{0} & \mathbf{K}_{LR}^D \Gamma_{RL} \end{bmatrix} = \left[\hat{\mathbf{K}}_L\right]^T \tag{16}$$

In these expression Γ_{RL} is the rotation matrix that allows the dependent cyclic boundary (*R*) DOFs of sector *j* to be expressed as a function of the independent (*L*) DOFs of sector *j+1* in a local frame of reference.

The remaining blocks of Eq. (14) take the following forms:

$$\widetilde{\mathbf{K}}_{\chi I_i}^{D_j} = \begin{bmatrix} \mathbf{K}_{CI_i}^D & \mathbf{0} \\ \mathbf{K}_{LI_i}^D + \Gamma_{RL}^T \mathbf{K}_{RI_i}^D \cos\left((j-1)\alpha\right) & \Gamma_{RL}^T \mathbf{K}_{RI_i}^D \sin\left((j-1)\alpha\right) \\ \mathbf{0} & \mathbf{K}_{CI_i}^D \\ -\Gamma_{RL}^T \mathbf{K}_{RI_i}^D \sin\left((j-1)\alpha\right) & \mathbf{K}_{LI_i}^D + \Gamma_{RL}^T \mathbf{K}_{RI_i}^D \cos\left((j-1)\alpha\right) \end{bmatrix} \tag{17}$$

$$\widetilde{\mathbf{K}}_{I_i I_i}^{D_j} = \begin{bmatrix} \mathbf{K}_{I_i I_i}^D & \mathbf{0} \\ \mathbf{0} & \mathbf{K}_{I_i I_i}^D \end{bmatrix} \quad , \quad \widetilde{\mathbf{K}}_{I_1 I_2}^{D_j} = \begin{bmatrix} \mathbf{K}_{I_1 I_2}^D & \mathbf{0} \\ \mathbf{0} & \mathbf{K}_{I_1 I_2}^D \end{bmatrix} \tag{18}$$

The expressions for the single harmonics blocks $\widetilde{\mathbf{K}}_m^{D_1}$, and when *N* is even, $\widetilde{\mathbf{K}}_m^{D_W}$ are:

$$\widetilde{\mathbf{K}}_m^{D_{(1,W)}} = \begin{bmatrix} \widetilde{\mathbf{K}}_{\eta\eta}^{D_{(1,W)}} & \widetilde{\mathbf{K}}_{\eta I_1}^{D_{(1,W)}} & \widetilde{\mathbf{K}}_{\eta I_2}^{D_{(1,W)}} \\ & \widetilde{\mathbf{K}}_{I_1 I_1}^{D_{(1,W)}} & \widetilde{\mathbf{K}}_{I_1 I_2}^{D_{(1,W)}} \\ sym & & \widetilde{\mathbf{K}}_{I_2 I_2}^{D_{(1,W)}} \end{bmatrix} = \begin{bmatrix} \widetilde{\mathbf{K}}_{\eta\eta}^{D_{(1,W)}} & \widetilde{\mathbf{K}}_{\eta I_1}^{D_{(1,W)}} & \widetilde{\mathbf{K}}_{\eta I_2}^{D_{(1,W)}} \\ & \mathbf{K}_{I_1 I_1}^D & \mathbf{K}_{I_1 I_2}^D \\ sym & & \mathbf{K}_{I_2 I_2}^D \end{bmatrix} \tag{19}$$

With:

$$\widetilde{\mathbf{K}}_{\eta\eta}^{D_{(1,W)}} = \begin{bmatrix} \mathbf{K}_{CC}^D & \mathbf{K}_{CL}^D\ (+,-)\,\mathbf{K}_{CR}^D \Gamma_{RL} \\ Sym & \mathbf{K}_{LL}^D + \Gamma_{RL}^T \mathbf{K}_{RR}^D \Gamma_{RL}\ (+,-)\,\mathbf{K}_{LR}^D \Gamma_{RL}\ (+,-)\,\Gamma_{RL}^T \mathbf{K}_{RL}^D \end{bmatrix}$$
$$\widetilde{\mathbf{K}}_{\eta I_i}^{D_{(1,W)}} = \begin{bmatrix} \mathbf{K}_{CI_i}^D \\ \mathbf{K}_{LI_i}^D\ (+,-)\,\Gamma_{RL}^T \mathbf{K}_{RI_i}^D \end{bmatrix} \tag{20}$$

2.3 Craigh-Bampton cyclic disk component

In the previous section the disk matrices via cyclic symmetry were presented. However, in order to obtain a ROM of the impeller, the model of the disk must be also reduced. Consequently, the Craig and Bampton formulation using the real cyclic formulation is implemented here.

The real cyclic physical displacements of the disk are expressed in the reduced modal space for each harmonic *j*, by virtue of a modal matrix, as:

$$\widetilde{\mathbf{u}}^{D_j} = \begin{Bmatrix} \widetilde{\mathbf{u}}_{\chi}^{D_j} \\ \widetilde{\mathbf{u}}_{I_1}^{D_j} \\ \widetilde{\mathbf{u}}_{I_2}^{D_j} \end{Bmatrix} = \begin{bmatrix} \widetilde{\Phi}_{\chi\xi}^{D_j} & \widetilde{\Psi}_{\chi I_1}^{D_j} & \widetilde{\Psi}_{\chi I_2}^{D_j} \\ \mathbf{0} & \mathbf{I}_{I_1} & \mathbf{0} \\ \mathbf{0} & \mathbf{0} & \mathbf{I}_{I_2} \end{bmatrix} \begin{Bmatrix} \widetilde{\mathbf{p}}_{\xi}^{D_j} \\ \widetilde{\mathbf{p}}_{I_1}^{D_j} \\ \widetilde{\mathbf{p}}_{I_2}^{D_j} \end{Bmatrix} = \widetilde{\mathbf{H}}^{D_j} \widetilde{\mathbf{p}}^{D_j} \tag{21}$$

Note that in this formulation the physical and modal coordinates representing the interface DOFs are the same, while the internal physical DOFs (*C*) are represented by a reduced set of modal coordinates (ξ). The block $\widetilde{\Phi}_{\chi\xi}^{D_j}$ represent a set of ξ fixed interface normal modes, while $\Psi_{\chi I_i}^{D_j}$ represent a set of I_i static interface attachment modes for blade *i*.

In this formulation the physical and modal coordinates representing the interface DOFs are the same, while the internal physical DOFs (*C*) are represented by a reduced set of modal coordinates (*q*). The blocks $\widetilde{\Psi}_{\chi I_i}^{D_j} = -\left[\widetilde{\mathbf{K}}_{\chi\chi}^{D_j}\right]^{-1} \widetilde{\mathbf{K}}_{\chi I_i}^{D_j}$ represent a set of I_i static constraint modes, while $\widetilde{\Phi}_{\chi\xi}^{D_j} = \left[\widetilde{\boldsymbol{\varphi}}_{\chi 1}^{D_j} \cdots \widetilde{\boldsymbol{\varphi}}_{\chi\xi}^{D_j}\right]$ represent a set of ξ fixed interface normal modes computed from the fixed interface eigenproblem of the disk sector:

$$\widetilde{\mathbf{K}}_{\chi\chi}^{D_J} \widetilde{\boldsymbol{\varphi}}_{\chi r}^{D_J} = \omega_r^2 \widetilde{\mathbf{M}}_{\chi\chi}^{D_J} \widetilde{\boldsymbol{\varphi}}_{\chi r}^{D_J} \qquad r = 1, \cdots, \xi \tag{22}$$

Transformation by way of the modal matrix $\widetilde{\mathbf{H}}^{D_j}$ yields reduced mass and stiffness matrices for the disk in real cyclic coordinates:

$$\widetilde{\mathbf{k}}^{\mathcal{D}} = \underset{j=1\cdots N}{\mathrm{Bdiag}}\left(\left[\widetilde{\mathbf{H}}^{D_j}\right]^T \widetilde{\mathbf{K}}^{D_j} \widetilde{\mathbf{H}}^{D_j}\right) = \underset{j=1\cdots N}{\mathrm{Bdiag}}\left(\begin{bmatrix} \Lambda_{\xi}^{D_j} & \mathbf{0} & \mathbf{0} \\ & \widetilde{\mathbf{k}}_{I_1 I_1}^{D_j} & \widetilde{\mathbf{k}}_{I_1 I_2}^{D_j} \\ \textit{Sym} & & \widetilde{\mathbf{k}}_{I_2 I_2}^{D_j} \end{bmatrix}\right) \tag{23}$$

$$\widetilde{\mathbf{m}}^{\mathcal{D}} = \underset{j=1\cdots N}{\mathrm{Bdiag}}\left(\left[\widetilde{\mathbf{H}}^{D_j}\right]^T \widetilde{\mathbf{M}}^{D_j} \widetilde{\mathbf{H}}^{D_j}\right) = \underset{j=1\cdots N}{\mathrm{Bdiag}}\left(\begin{bmatrix} \mathbf{I}_{\xi} & \widetilde{\mathbf{m}}_{\xi I_1}^{D_j} & \widetilde{\mathbf{m}}_{\xi I_2}^{D_j} \\ & \widetilde{\mathbf{m}}_{I_1 I_1}^{D_j} & \widetilde{\mathbf{m}}_{I_1 I_2}^{D_j} \\ \textit{Sym} & & \widetilde{\mathbf{m}}_{I_2 I_2}^{D_j} \end{bmatrix}\right) \tag{24}$$

Where:

$$\begin{aligned} \widetilde{\mathbf{k}}_{I_i I_i}^{D_j} &= \widetilde{\mathbf{K}}_{I_i \chi}^{D_j} \widetilde{\Psi}_{\chi I_i}^{D_j} + \widetilde{\mathbf{K}}_{I_i I_i}^{D_j} \\ \widetilde{\mathbf{k}}_{I_1 I_2}^{D_j} &= \widetilde{\mathbf{K}}_{I_1 \chi}^{D_j} \widetilde{\Psi}_{\chi I_2}^{D_j} + \widetilde{\mathbf{K}}_{I_1 I_2}^{D_j} \\ \widetilde{\mathbf{m}}_{\xi I_i}^{D_j} &= \left[\widetilde{\Phi}_{\chi\xi}^{D_j}\right]^T \left[\widetilde{\mathbf{M}}_{\chi\chi}^{D_j} \widetilde{\Psi}_{\chi I_i}^{D_j} + \widetilde{\mathbf{M}}_{\chi I_i}^{D_j}\right] \\ \widetilde{\mathbf{m}}_{I_i I_i}^{D_j} &= \left[\widetilde{\Psi}_{\chi I_i}^{D_j}\right]^T \left[\widetilde{\mathbf{M}}_{\chi\chi}^{D_j} \widetilde{\Psi}_{\chi I_i}^{D_j} + \widetilde{\mathbf{M}}_{\chi I_i}^{D_j}\right] + \widetilde{\mathbf{M}}_{I_i \chi}^{D_j} \widetilde{\Psi}_{\chi I_i}^{D_j} + \widetilde{\mathbf{M}}_{I_i I_i}^{D_j} \\ \widetilde{\mathbf{m}}_{I_1 I_2}^{D_j} &= \left[\widetilde{\Psi}_{\chi I_1}^{D_j}\right]^T \left[\widetilde{\mathbf{M}}_{\chi\chi}^{D_j} \widetilde{\Psi}_{\chi I_2}^{D_j} + \widetilde{\mathbf{M}}_{\chi I_2}^{D_j}\right] + \widetilde{\mathbf{M}}_{I_1 \chi}^{D_j} \widetilde{\Psi}_{\chi I_2}^{D_j} + \widetilde{\mathbf{M}}_{I_1 I_2}^{D_j} \end{aligned} \tag{25}$$

Finally, matrices expressed in the non-cyclic reduced coordinates are obtained through the following transformation:

$$\mathbf{k}^{\mathcal{D}} = \left(\mathbf{F}_N \otimes \mathbf{I}_{(\xi + I_1 + I_2)}\right) \widetilde{\mathbf{k}}^{\mathcal{D}} \left(\mathbf{F}_N^T \otimes \mathbf{I}_{(\xi + I_1 + I_2)}\right) = \begin{bmatrix} \mathbf{k}_{SS}^{\mathcal{D}} & \mathbf{0} \\ \mathbf{0} & \mathbf{k}_{YY}^{\mathcal{D}} \end{bmatrix} \tag{26}$$

$$\mathbf{m}^{\mathcal{D}} = \left(\mathbf{F}_N \otimes \mathbf{I}_{(\xi+I_1+I_2)}\right)\widetilde{\mathbf{m}}^{\mathcal{D}}\left(\mathbf{F}_N^T \otimes \mathbf{I}_{(\xi+I_1+I_2)}\right) = \begin{bmatrix} \mathbf{I}_S & \mathbf{m}_{SY}^{\mathcal{D}} \\ \mathbf{m}_{YS}^{\mathcal{D}} & \mathbf{m}_{YY}^{\mathcal{D}} \end{bmatrix} \tag{27}$$

Where $S = N(\xi)$ and $Y = N(I_1 + I_2)$.

2.4 Impeller reduced-order model

In order to obtain the impeller ROM, the vector of modal coordinates is ordered to obtain:

$$\mathbf{p}^{\mathcal{G}} = \begin{Bmatrix} \mathbf{p}_Q^{\mathcal{A}} \\ \mathbf{p}_S^{\mathcal{D}} \\ \mathbf{p}_Y^{\mathcal{A},\mathcal{D}} \end{Bmatrix} \tag{28}$$

Therefore the stiffness and mass matrices for the whole impeller are given by:

$$\mathbf{k}^{\mathcal{G}} = \begin{bmatrix} \Lambda_Q^{\mathcal{A}} & \mathbf{0} & \mathbf{0} \\ & \mathbf{k}_{SS}^{\mathcal{D}} & \mathbf{0} \\ Sym & & \mathbf{k}_{YY}^{\mathcal{A}} + \mathbf{k}_{YY}^{\mathcal{D}} \end{bmatrix} \quad , \quad \mathbf{m}^{\mathcal{G}} = \begin{bmatrix} \mathbf{I}_Q & \mathbf{0} & \mathbf{m}_{QY}^{\mathcal{A}} \\ & \mathbf{I}_S & \mathbf{m}_{SY}^{\mathcal{D}} \\ Sym & & \mathbf{m}_{YY}^{\mathcal{A}} + \mathbf{m}_{YY}^{\mathcal{D}} \end{bmatrix} \tag{29}$$

The impeller ROM equation of motion may be written as:

$$\mathbf{m}^{\mathcal{G}}\ddot{\mathbf{p}}^{\mathcal{G}} + \mathbf{k}^{\mathcal{G}}\mathbf{p}^{\mathcal{G}} = \mathbf{f}^{\mathcal{G}} \tag{30}$$

Where the modal force vector $\mathbf{f}^{\mathcal{G}}$ has the form:

$$\mathbf{f}^{\mathcal{G}} = \begin{Bmatrix} \mathbf{f}_Q^{\mathcal{A}} \\ \mathbf{f}_S^{\mathcal{D}} \\ \mathbf{f}_Y^{\mathcal{A},\mathcal{D}} \end{Bmatrix} \tag{31}$$

Considering that dynamic forces are only applied to the blades' internal DOFs, *i.e.* no forces are applied to the blade-disk interface or to the disk, the modal force vector may be expressed in function of the forces applied only to the *C* DOFs of the blades:

$$\mathbf{f}^{\mathcal{G}} = \begin{Bmatrix} \mathbf{f}_Q^{\mathcal{A}} \\ \mathbf{f}_S^{\mathcal{D}} \\ \mathbf{f}_Y^{\mathcal{A},\mathcal{D}} \end{Bmatrix} = \begin{bmatrix} \mathbf{I}_N \otimes \begin{bmatrix} \left[\Phi_{Cq}^{A_1}\right]^T & \mathbf{0} \\ \mathbf{0} & \left[\Phi_{Cq}^{A_2}\right]^T \end{bmatrix} \\ \mathbf{0} \\ \mathbf{I}_N \otimes \begin{bmatrix} \left[\Phi_{Cq}^{A_1}\right]^T & \mathbf{0} \\ \mathbf{0} & \left[\Phi_{Cq}^{A_2}\right]^T \end{bmatrix} \end{bmatrix} \begin{Bmatrix} \begin{Bmatrix} \mathbf{f}_C^{A_1} \\ \mathbf{f}_C^{A_2} \end{Bmatrix}_{j=1} \\ \begin{Bmatrix} \mathbf{f}_C^{A_1} \\ \mathbf{f}_C^{A_2} \end{Bmatrix}_{j=2} \\ \vdots \\ \begin{Bmatrix} \mathbf{f}_C^{A_1} \\ \mathbf{f}_C^{A_2} \end{Bmatrix}_{j=N} \end{Bmatrix} \tag{32}$$

2.5 Mistuning introduction

Mistuning is modeled as variations in the modal stiffnesses of each cantilevered blade as:

$$\overline{\Lambda}_{r,j}^{A_i} = \Lambda_{r,j}^{A_i}\left(1 + \delta_{r,j}^{A_i}\right) \tag{33}$$

Where $\Lambda_{r,j}^{A_i}$ is the modal stiffness (*i.e.* square natural frequency) of the r^{th} natural mode of

the blade type i on the j^{th} sector, and $\delta_{r,j}^{A_i}$ is the corresponding mistuning parameter.

Modal stiffness of all blades in the impeller $\Lambda_Q^{\mathcal{A}}$ appear explicitly in Eq. (29) grouped in a diagonal matrix. Hence, mistuning is introduced directly in the global stiffness matrix as follows:

$$\overline{\Lambda}_Q^{\mathcal{A}} = \Lambda_Q^{\mathcal{A}}\left(\mathbf{I}_Q + \mathrm{B}\mathrm{diag}\left(\begin{bmatrix}\mathrm{diag}(\delta_{r,j}^{A_1}) & \mathbf{0}\\ \mathbf{0} & \mathrm{diag}(\delta_{r,j}^{A_2})\end{bmatrix}\right)\right) \tag{34}$$

This formulation permits to introduce different mistuning patterns for each blade type of the impeller, that is to say different mistuning values for each retained mode in any blade.

3 REDUCED ORDER MODELLING VALIDATION

In to order validate the methodology proposed in the previous section a comparison of the predictions obtained by means of the impeller ROM, relative to the parent finite element model, is presented. First, tuned and mistuned free response natural frequencies and mode shapes are evaluated. Next, the tuned and mistuned forced response blade amplitudes to a harmonic excitation are studied.

3.1 Model description

A simplified impeller model, shown in Figure 2 is used in this work for validation purposes. The impeller is formed by ten sectors with two blade types. Blade type 1 (main blade) is 100 mm long, while blade type 2 (splitter blade) is only 70 mm long, and both are uniformly twisted 15 degrees along the length. The disk is 16.7 mm thick and has an outer diameter of 420 mm with an inner diameter of 200 mm. The disk is assumed to be fixed to the ground at the inner diameter. The material properties used for the whole impeller are those of steel (E = 200 GPa, ρ = 7.820 kg/m^3 and ν = 0.3).

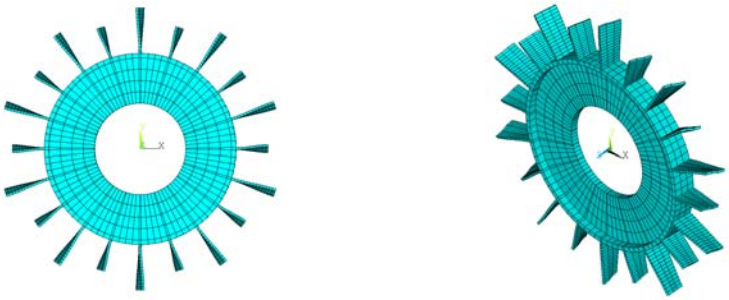

(a) (b)

Figure 2: Impeller FE model: a) frontal view; b) isometric view

All finite element modeling was done in ANSYS$^{\text{TM}}$. Both, the disk and all the blades are modeled using eight-node brick elements with 3 DOFs per node. The disk sector consists of 70 elements, and each blade, disregarding the type, has 42 elements. There are a total of 10970 DOFs in the finite element model. The simplified geometry of the model and the relatively coarse mesh does not represent an industrial impeller; however this is not a major concern for this study, since the main goal is to compare the behavior of the impeller ROM, relative to its parent finite element. Mistuning in the finite element model is introduced by modifying the Young's modulus of each blade type as:

$$E_j^{A_1} = E_0\left(1+\delta_j^{A_1}\right) \tag{35}$$

This implies that all the cantilevered frequencies of a blade type in a sector are modified with the same mistuning parameter; therefore it results in a two random mistuning patterns (one pattern for each blade type). In order to have a consistent mistuning on the ROM Eq. (34) is modified as:

$$\overline{\Lambda}_Q^{\mathcal{A}} = \Lambda_Q^{\mathcal{A}}\left(\mathbf{I}_Q + \mathrm{Bdiag}\left(\begin{bmatrix}\mathrm{diag}(\delta_j^{A_1}) & \mathbf{0}\\ \mathbf{0} & \mathrm{diag}(\delta_j^{A_2})\end{bmatrix}\right)\right) \tag{36}$$

The two random mistuning patterns used throughout this paper are listed in Table 1, and they were sampled from two uniform distributions of null mean and standard deviation 3.0% and 1.0%, respectively.

Sector (j)	Blade type 1 $\left(\delta_j^{A_1}\right)$	Blade type 2 $\left(\delta_j^{A_2}\right)$
1	0.012042639177694	-0.017125377549410
2	0.072236389651782	-0.014459594164888
3	-0.031032644357239	0.008079271023132
4	-0.011010563796759	-0.016195617223108
5	-0.090935145174010	0.022381962401530
6	-0.065870063107022	0.033303774580815
7	0.033212844640039	0.015887166666464
8	-0.034510884978526	-0.010772486716066
9	0.081291172118197	0.005800783996213
10	-0.077896339516871	-0.027063937948182

Table 1: Random mistuning patterns.

On the other hand, the impeller ROM was obtained by retaining 6 normal fixed interface modes to represent each blade type (*i.e.* $q_1 = q_2 = 6$), and 10 modal branches to represent the disk internal DOFs ($\xi = 10$), for a total of 700 DOFs. Therefore the impeller ROM size is 6.4% of the finite element parent model size.

3.2 Free response: tuned impeller

Figure 3a shows natural tuned frequencies *vs*. mode numbers. The figure clearly shows a close match between the ROM and the FEM predictions for the first 120 natural frequencies. It's important to notice that the ROM reproduces the pairs of repeated frequencies typical of cyclic symmetric structures. Figure 3b shows that the maximum relative error in the first 120 natural frequencies is less than 5%. Due to Rayleigh's quotient properties, relative error in frequencies may be misguiding for assessing the precision of the method regarding mode shapes, thus Figure 4a shows the Modal Assurance Criterion (MAC) for the first 120 mode shapes of the impeller, while Figure 4b show the form of 29th mode which has a MAC=77.3%, very close to the mean value of the MAC for the first 120 modes (MAC=76.5%).

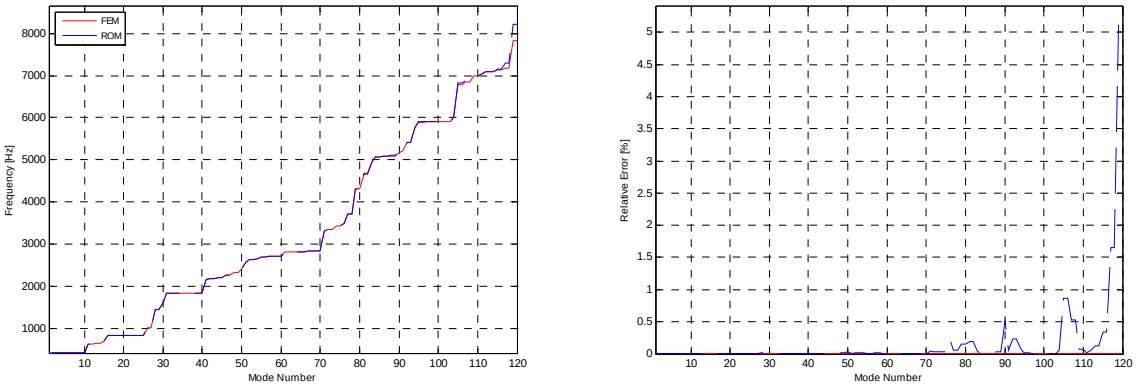

(a) (b)

Figure 3: Free tuned response: a) Natural frequencies; b) Relative error in frequency *vs*. mode

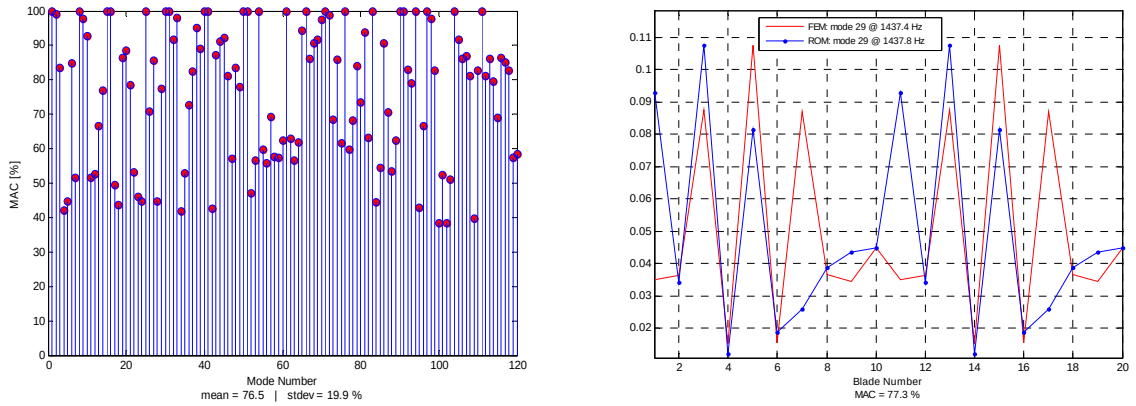

(a) (b)

Figure 4: Free tuned response: a) MAC vs. mode; b) 29th mode

The low value for the mean of the MAC obtained for the first 120 natural modes (76.5%) and the high value of standard deviation (19.9%) is explained because a shifting in the mode is present between the FE model and the ROM. This shifting is produced because being all the blades of the same type in the tuned impeller identical and the modes cyclic symmetric, there is no way to assure that a particular blade in the FE model correspond to a particular blade in the ROM, so a shifting between ROM and the FE parent model is possible. Figure 5 shows this shifting for a particular mode. In the next section where mistuning is introduced, a significant improvement of the mean and standard deviation of the MAC is obtained.

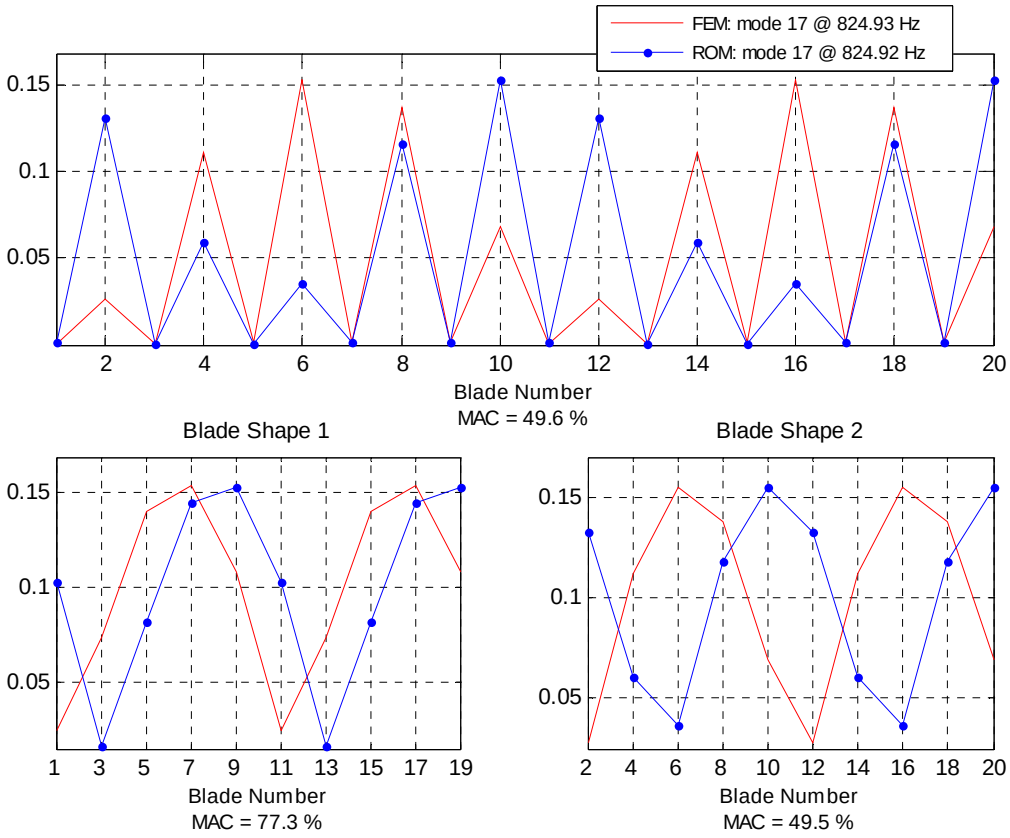

Figure 5: Free tuned response: shifting within a mode

3.3 Free response: mistuned impeller

Figure 6a presents natural mistuned frequencies *vs*. mode numbers, showing a close match between the ROM and the FEM predictions for the first 120 natural mistuned frequencies. It's important to notice that the ROM reproduces well the splitting of frequency pairs typical of mistuned cyclic structures. Figure 6b shows that the maximum relative error in the first 120 natural frequencies is less than 5.3%. As in the previous subsection, relative error in frequency may be misguiding for assessing the precision of the method regarding mode shapes, then Figure 7a shows the Modal Assurance Criterion (MAC) for the first 120 mode of the impeller, where a mean value of 93.4% and a standard deviation of 13.07% are obtained. These values are much better than those obtained for the tuned impeller (*cf*. Figure 4a). In order to have an idea of how good or bad looks a mode shape with a MAC close to the mean value, Figure 7b show the form of the 55^{th} mode, who has a MAC just under the mean value. From this figure is obvious that the impeller ROM captures well the general form and amplitudes of the mode. Regarding localized modes, Figure 8 shows the 38^{th} natural mode which presents high localization and a MAC=99.9%. It is important to notice that all localized modes have MAC values close to 100%, thus proving that the ROM captures very well this important phenomenon.

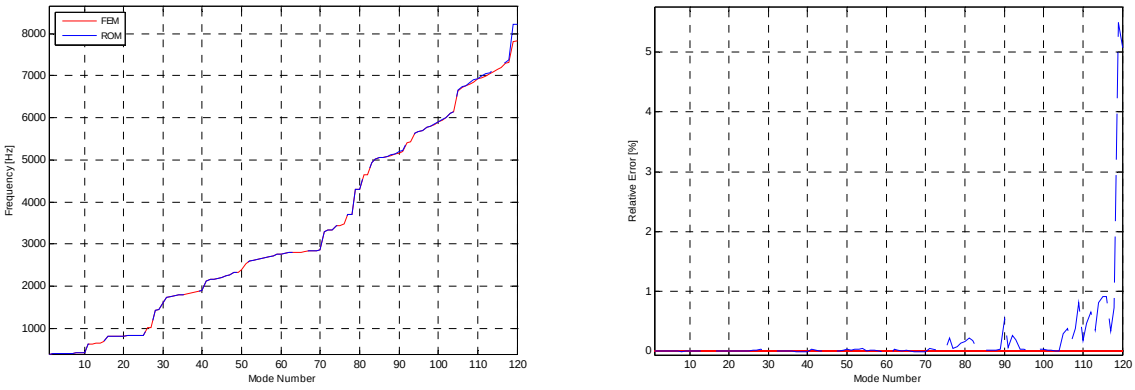

(a) (b)

Figure 6: Free mistuned response: a) Natural frequencies; b) Relative error in frequencies.

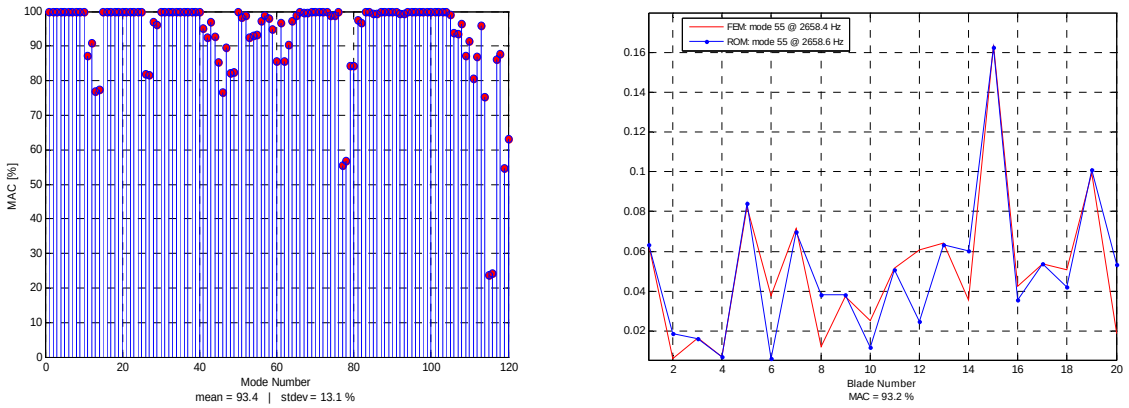

(a) (b)

Figure 7: Free mistuned response: a) MAC vs. mode; b) 55th mode

3.4 Forced response: tuned impeller

In this section the accuracy of the reduced order model for predicting forced response blade amplitudes is investigated. In this analysis structural damping for the rotor is included, and a harmonic excitation that differs only in phase from blade to blade is assumed. Forced response amplitudes are then obtained as solutions of the following problem:

$$\mathbf{m}^{\mathcal{G}}\ddot{\mathbf{p}}^{\mathcal{G}} + \mathbf{k}^{\mathcal{G}}\left(1+\mu\sqrt{-1}\right)\mathbf{p}^{\mathcal{G}} = \mathbf{f}_0 e^{\sqrt{-1}\left(\Omega t+\theta_k^{A_i}\right)} \tag{37}$$

Where μ is the structural damping coefficient, Ω is the excitation frequency, and $\theta_k^{A_i}$ the phase at blade number k of type A_i given by:

$$\begin{aligned} \theta_k^{A_1} &= \frac{2\pi M_0}{N}(k-1) \\ \theta_k^{A_2} &= \frac{2\pi M_0}{N}(k-0.5) \end{aligned} \tag{38}$$

With M_0 the engine order of the excitation.

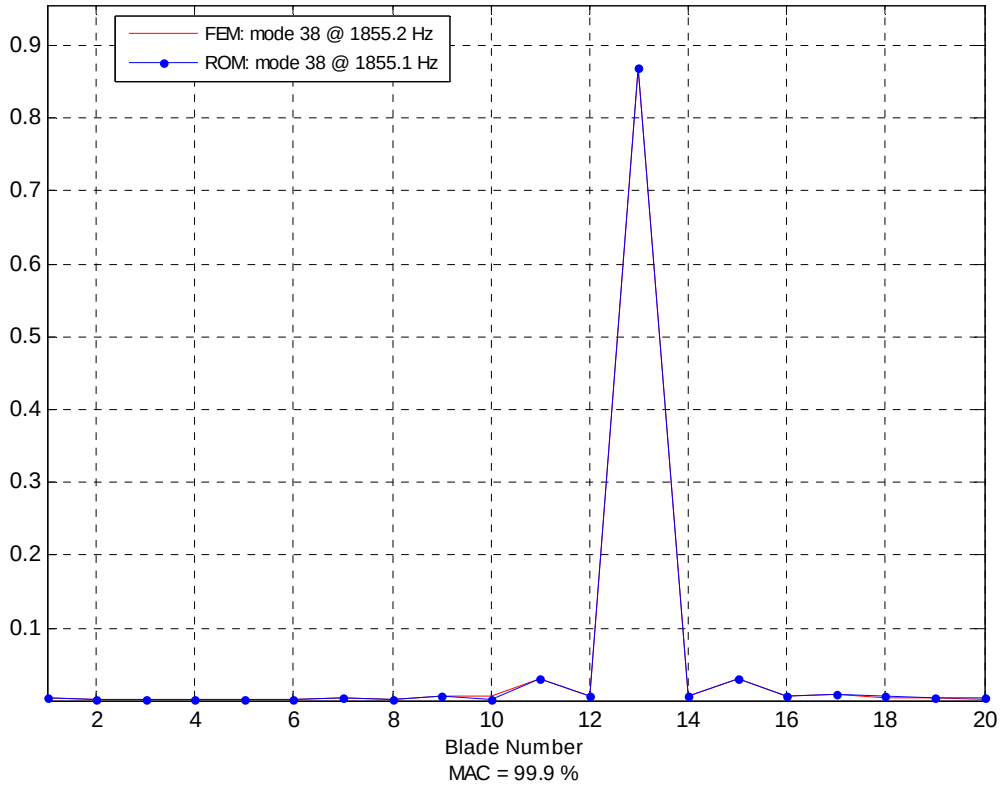

Figure 8: Free mistuned response: 38th mode (highly localized)

For both, FE and reduced order model, a structural damping coefficient of 0.5% was used. The excitation force was applied to all nodes at the tip of each blade, acting on the axial and tangential directions. The resulting force in each blade has unitary amplitude. Results are presented for an excitation of engine order three (M_0 = 3) for both, the tuned and mistuned case, and for a frequency range from 10Hz to 3200Hz with a step of 10 Hz.

Figure 9a shows the maximum blade displacement norm of the tuned forced response for the frequency range under study (*i.e.* all blade displacement norms are calculated for a given forcing frequency and the maximum values for each frequency are then plotted in the figure). This figure shows that the ROM predicts very well the forcing response of the tuned impeller (resonances and amplitudes).

Other way to evaluate the ability of the ROM to predict the forced response is by means of the calculation of a MAC for the blade displacement norms obtained for each forcing frequency (*i.e.* the displacement norm of each blade is calculated for a given frequency, and these values are considered a vector, thus permitting the calculation of a MAC). This procedure was applied and is presented in Figure 9b, showing that for the tuned case, the ROM captures very well the forced response.

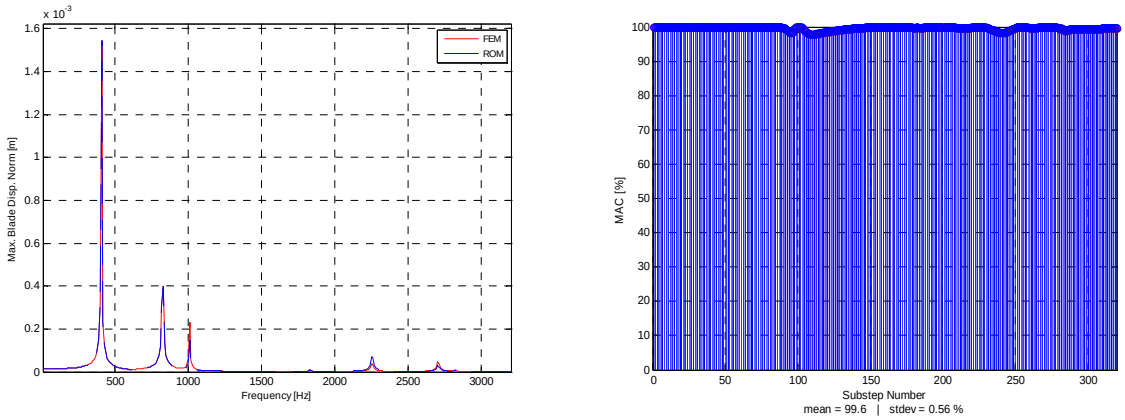

(a) (b)

Figure 9: Forced tuned response: a) Global displacement norm; b) MAC

To have an idea of the form of the forced response, Figure 10 shows the values of the displacement norm for each blade corresponding to the forced response at a frequency of 410 Hz. The agreement between FE model and ROM is excellent. Note that blade type 2 (splitter) have displacement norms smaller than blade type 1 (the main).

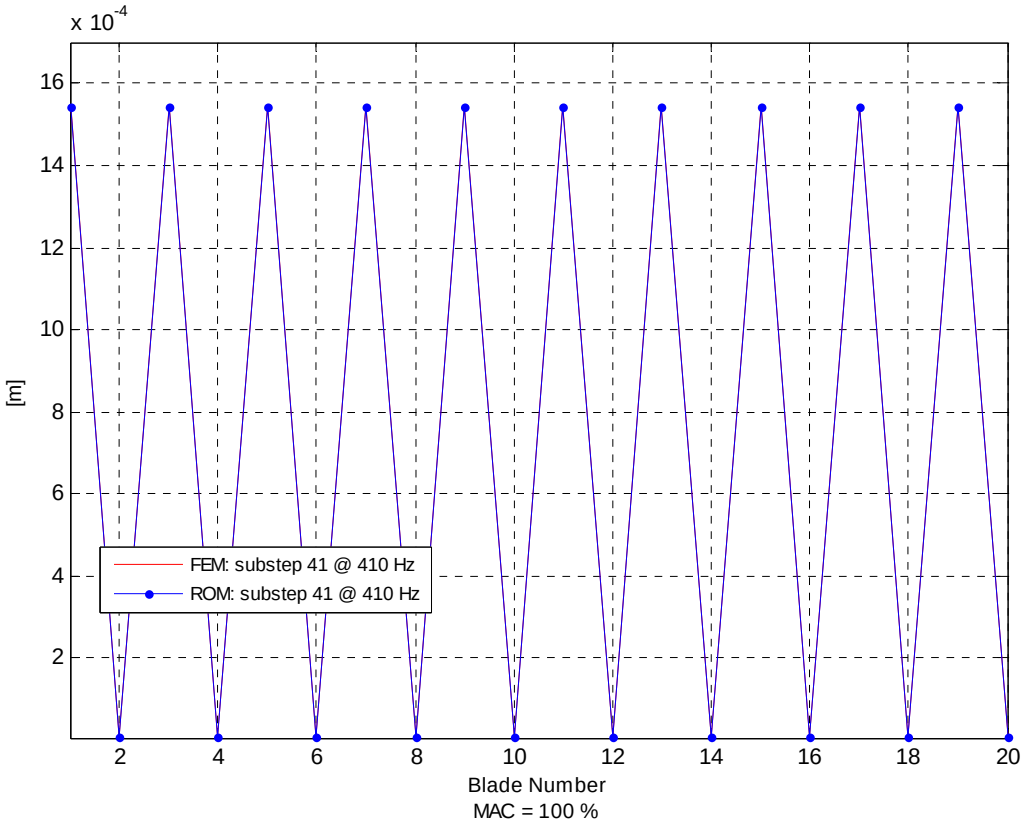

Figure 10: Forced tuned response @ 410 Hz

3.5 Forced response: mistuned impeller

Figure 11a shows the maximum blade displacement norm of the mistuned forced response for the frequency range under study (*i.e.* all blade displacement norms are calculated for a given forcing frequency and the maximum values for each frequency are then plotted in the figure). This figure shows that the ROM predicts very well the forcing response of the tuned impeller (frequencies and amplitudes of resonances). Note also that mistuning applied modifies the forced response when compared to the tuned forced response of the impeller (*cf.* Figure 9a) producing an increase of resonant amplitudes and the apparition of new resonances.

As in the case of the tuned impeller, the MAC calculated for the vector of blade displacement norms, obtained for each forcing frequency, is presented in Figure 11b. These results show an excellent agreement between the ROM and FE model predictions (mean value close to 98.4% and a standard deviation of only 2.66%).

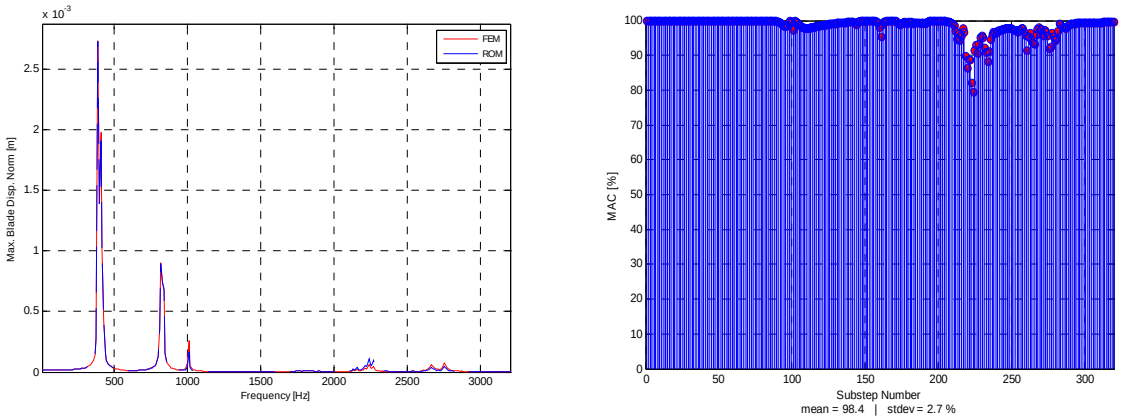

(a) (b)

Figure 11: Forced tuned response: a) Global displacement norm; b) MAC

Figure 12 shows the values of the displacement norm for each blade of the impeller corresponding to the mistuned forced response at a frequency of 390 Hz. The agreement between ROM and FE model is excellent, even in the case where a localized response is present.

4 CONCLUSIONS

This paper presents a methodology to obtain the ROM of an impeller incorporating splitter blades. The methodology is based in a component mode synthesis approach permitting to introduce different mistuned patterns for each blade type (main and splitter). The proposed methodology was applied to a simplified impeller model and comparison for the free and forced responses of the tuned and mistuned impeller where presented. From these results the following conclusions may be drawn:

The reduced order model may be used effectively in the calculation of free and forced response for both tuned and mistuned impellers. In particular, repeated frequencies, frequency unfolding, mode and response localization and maximal blade response are features well captured and predicted by the reduced model.

The Modal Assurance Criterion seems to be an effective and relatively simple way to

evaluate the performance of an impeller ROM respect the FE parent model. The high mean values and the relatively small standard deviations observed, except for the tuned free response, prove that the ROM predicts fairly well the free and force response of the FE parent model.

Future works include the application of this methodology to an industrial impeller, and the inclusion of a secondary reduction of the blade-disk interface DOFs, whose number may be too large in the case of an industrial impeller, in order to obtain a smaller ROM.

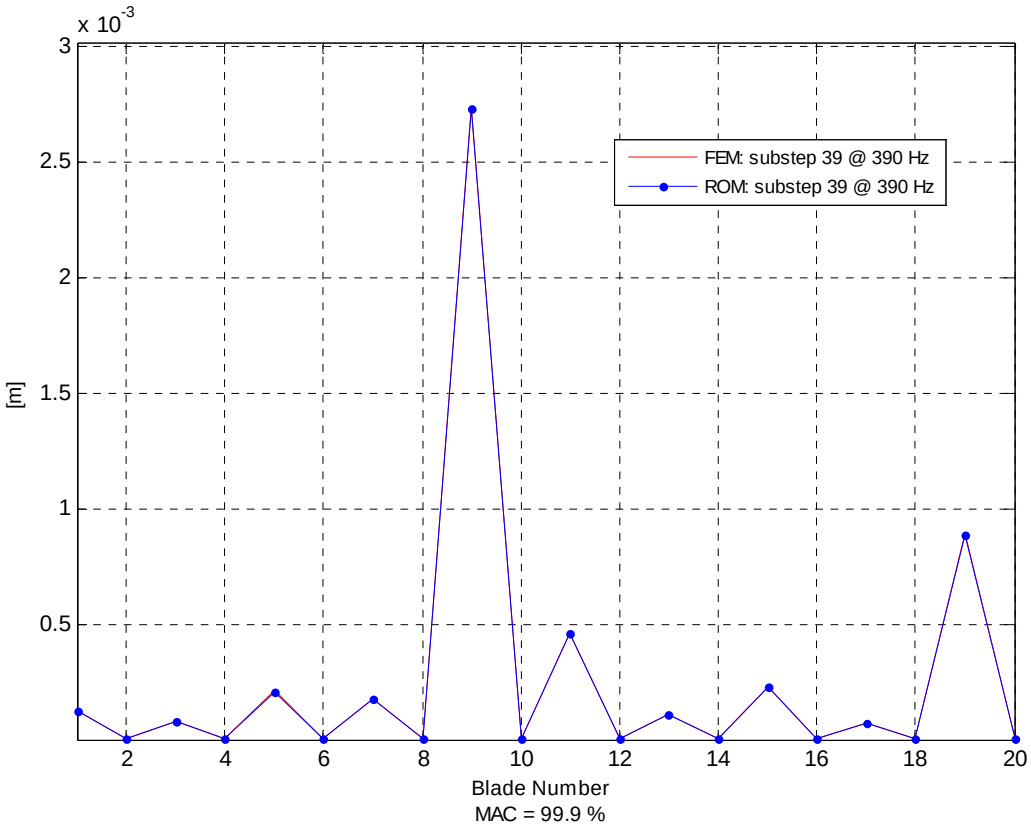

Figure 12: Forced mistuned response @ 390 Hz

REFERENCES

Bladh, R., Castanier, M., and Pierre, C., Component-mode-based reduced order modeling techniques for mistuning bladed disks - Part I: Theoretical models, *ASME Journal of Engineering for Gas Turbines and Power*, 123:89-99, 2001.

Boulton, L. A., Casanova, E., Reduced order model for a two stage gas turbine including mistuned bladed disks and shaft interaction, *Proceeding of ASME Turbo Expo 2009, Power for Land, Sea and Air, June 8-12, Orlando, Florida, USA*, GT2009-59335, 2009.

Casanova, E., Dynamique des structures cycliques avec incertitudes: Modélisation modales des aubages de turbines. *PhD thesis, Université de Technologie de Compiègne*, 2002.

Craig, R. R., Jr., and Bampton, M. C. C., Coupling of substructures for dynamic analyses, *AIAA Journal*, 6:1313-1319, 1968.

Laxalde, D., Thouverez, F., and Lombard, J., Dynamics of multi-stage bladed disks systems, *Proceeding of ASME Turbo Expo 2007*, *Power for Land, Sea and Air, May 14-17, Montreal, Canada*, GT2007-27083, 2007.

Patel, B., Nagpal, V., Srivastava, R., Lentz, j., and Kerner, K., Probabilistic mistuning analysis and estimation of HCF life of a honeywell impeller, *Proceeding of the ninth biennial ASCE aerospace division international conference on engineering, construction and operations in challenging environments*, 476-483, 2004.

Petrov, E., Sanliturk, K., and Ewins, D., A new method for dynamic analysis of mistuned bladed disks based on the exact relationship between tuned and mistuned systems, *ASME Journal of Engineering for Gas Turbines and Power*, 124:586-597, 2002.

Seguí, B., Casanova, E., Application of a reduced order modeling technique for mistuned bladed disk-shaft assemblies, *Proceeding of ASME Turbo Expo 2007, Power for Land, Sea and Air, May 14-17, Montreal, Canada*, GT2007-27594, 2007.

Sinha, A., Reduced-order model of a mistuned multi-stage blade rotor, *Proceeding of ASME Turbo Expo 2007, Power for Land, Sea and Air, May 14-17, Montreal, Canada*, GT2007-27277, 2007.

Song, S., Castanier, M., Pierre, C., Multi-Stage Modeling of Turbine Engine Rotor Vibration, In Proceedings of IDETC/CIE, DETC2005-85740, Long Beach, California, 1533-1543, 2005.

Ziaei-Rad, S., Finite element, modal testing and modal analysis of a radial flow impeller, *Iranian Journal of Science & Technology, Transaction B, Engineering*, 29: B2, 2005.